IOPscience iopscience.iop.org

Home Search Collections Journals About Contact us My IOPscience

Nanograins with 90° grain boundaries in high transition temperature superconducting films

This article has been downloaded from IOPscience. Please scroll down to see the full text article.

2003 J. Phys.: Condens. Matter 15 7925

(http://iopscience.iop.org/0953-8984/15/46/011)

View the table of contents for this issue, or go to the journal homepage for more

Download details:
IP Address: 171.66.16.125
The article was downloaded on 19/05/2010 at 17:45

Please note that terms and conditions apply.

INSTITUTE OF PHYSICS PUBLISHING JOURNAL OF PHYSICS: CONDENSED MATTER

J. Phys.: Condens. Matter **15** (2003) 7925–7937 PII: S0953-8984(03)69284-2

Nanograins with 90° grain boundaries in high transition temperature superconducting films

S V Bobylev, M Yu Gutkin and I A Ovid'ko

Institute for Problems of Mechanical Engineering, Russian Academy of Sciences, Bolshoj 61, Vasilievskii Ostrov, St Petersburg 199178, Russia

E-mail: ovidko@def.ipme.ru

Received 19 September 2003
Published 7 November 2003
Online at stacks.iop.org/JPhysCM/15/7925

Abstract

A theoretical model is suggested which describes a non-conventional relaxation mechanism in strained high transition temperature superconducting films, namely the formation of nanograins with 90° grain boundaries. It is theoretically revealed here that misfit stresses in superconducting thin films at early stages of their growth are effectively relaxed through the formation of nanograins with their crystal lattice misoriented by 90° relative to the crystal lattice of the film matrix. With increasing film thickness, the formation of a continuous layer resulting from the convergence of nanograins becomes energetically favourable. The results of the model account for experimental data on the observation of nanograins with 90° grain boundaries in YBaCuO films, reported in the literature.

1. Introduction

The high transition temperature (T_c) superconducting properties of cuprates are highly sensitive to the presence of grain and interphase boundaries; see, for example, [1–4]. In particular, grain boundaries drastically reduce the critical current density in polycrystalline high-T_c superconductors [1–3], while interphase boundaries create misfit stresses capable of strongly enhancing the transition temperature T_c in thin cuprate films [4]. The remarkable suppression of the transport properties of grain boundaries in high-T_c superconductors is the subject of controversial explanations (see, for example, [5–14]), which, however, come to an agreement that grain boundary structures crucially influence their transport properties. This causes an interest in structural transformations of grain boundaries experimentally detected in high-T_c superconductors; see, for example, [15–18]. Following theoretical models [19–21], these structural transformations are driven by internal stress fields of grain boundary dislocations and external misfit stresses generated at interphase film/substrate boundaries. For instance, lattice dislocations composing low-angle tilt boundaries often undergo splitting and amorphizing

 © 2003 IOP Publishing Ltd Printed in the UK

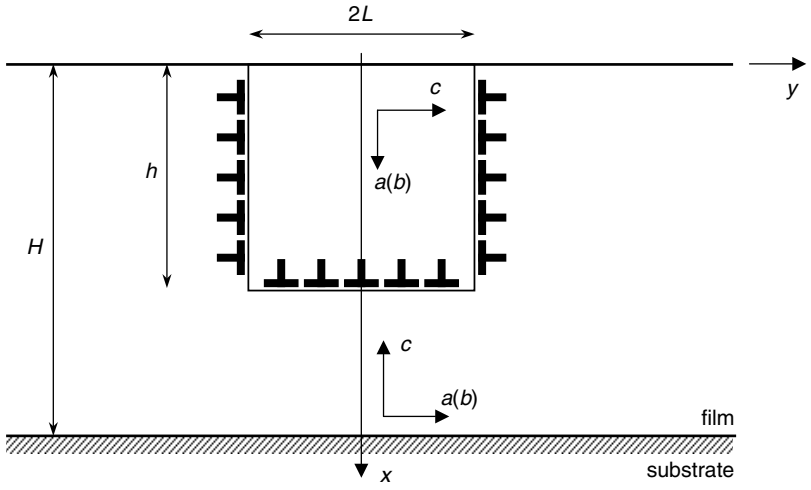

Figure 1. Lateral and bottom 90° tilt boundaries of nanograins are represented as ensembles of continuously distributed coherent dislocations in the case of coherent matching.

transformations (see experimental data [15–18] and theoretical models [19, 20]) under the action of dislocation stress fields, which definitely affect the critical current density across the boundaries.

Interphase boundaries create misfit stresses capable of causing structural transformations of grain boundaries [21] in high-T_c superconducting films. In this case, transformations of grain boundary structures serve as a misfit stress relaxation mechanism in strained films. Other relaxation mechanisms in high-T_c cuprate films are related to phase transformations and the conventional generation of misfit dislocations; see, for example, experimental data [22, 23] and a theoretical model [24]. Recently, it has been reported that nanoscale grains with 90° tilt boundaries (hereinafter denoted as nanograins) are intensively formed in YBaCuO films growing on $LaAlO_3$ substrates [25]. We treat this experimentally detected phenomenon as a new mechanism for relaxation of misfit stresses (occurring at interphase boundaries), being, in fact, a manifestation of the effects of interphase boundaries on both the generation and evolution of grain boundaries in high-T_c superconducting films. The main aim of this paper is to elaborate a theoretical model describing the formation of nanograins and their ensembles in growing high-T_c superconducting films as a misfit stress relaxation mechanism. In doing so, we will consider also the limiting case where nanograins converge into a continuous layer on the film top, separated by 90° boundary(ies) from the bottom film layer adjacent to the interphase (film/substrate) boundary.

2. 90° grain boundaries of nanograins in strained high-T_c superconducting films: model

Recently, nanoscale grains with 90° tilt boundaries (nanograins) have been experimentally observed [25] in high-T_c superconducting YBaCuO films growing on $LaAlO_3$ substrates. The crystal lattice of each nanograin is rotated by 90° relative to the crystal lattice of the surrounding material, the film matrix (figure 1). More precisely, Zhai *et al* [25] have experimentally examined YBaCuO films with the crystallographic axis *c* ([001] direction) perpendicular to the film/substrate boundary. Nanograins in these films have crystal lattices rotated by 90° relative to either the *a* or *b* crystallographic axes, in which cases the [100] and [010] crystallographic

directions of the nanograin crystal lattice are perpendicular to both the film free surface and the film/substrate boundary (figure 1). Following experimental data [25], nanograins having dimensions of the order of 10 nm are formed in a growing film at a distance ≈30–45 atomic layers from the film/substrate boundary and commonly are extended to the film free surface (figure 1). The boundaries between a nanograin and the film matrix are capable of being stress sources that compensate, in part, for misfit stresses. In this context, the formation of nanograins represents a new mechanism for relaxation of misfit stresses, which serves as an effective alternative to conventional relaxation mechanisms (see, for example, review articles [26–38]) related to the formation of misfit dislocations and their configurations in strained films.

Let us discuss in detail this relaxation mechanism in strained $YBa_2Cu_3O_{7-\delta}$ films. Crystal lattices of $YBa_2Cu_3O_{7-\delta}$ superconductors (and other high-T_c cuprates) are not cubic ones [39]. As a corollary, their matching at 90° grain boundaries is characterized by a dilatation misfit between crystal lattice parameters characterizing different crystallographic axes. For instance, let us consider a nanograin whose crystal lattice is rotated by 90° along the b axis relative to the film crystal lattice. Two lattices are matched at the nanograin boundaries, in which case the matched crystal lattice parameters a and c are very different. The value of $3a$ is close to c. In these circumstances, each four atomic layers of a nanograin, with the sum thickness $3a$, are matched with four atomic layers of the film matrix, characterized by thickness c (figure 2). Since $3a$ is slightly different from c, in the case discussed, the bottom grain boundary between a domain and the film matrix serves as a coherent interphase boundary characterized by the one-dimensional misfit parameter

$$f_1 = \frac{c/3 - a}{c/3}. \tag{1}$$

From the crystallography of a nanograin shown in figure 1 it follows that the lateral 90° grain boundaries of the nanograin serve as interphase boundaries with misfit parameter $\tilde{f}_2 = -f_1$.

In the case of coherent matching of crystal lattices at the bottom grain boundary, misfit stresses occurring at this boundary are effectively represented as those created by continuously distributed (along the boundary) edge dislocations with infinitesimal Burgers vectors $\mathrm{d}\boldsymbol{b}_c$. Such dislocations are called coherent dislocations and are characterized by the linear density ρ_c which is in the following relationship with the dislocation Burgers vector $\mathrm{d}\boldsymbol{b}_c$ and the misfit parameter f_1:

$$\rho_c \, \mathrm{d}b_c = f_1. \tag{2}$$

The misfit stresses inside the nanograin due to the coherent bottom boundary in the situation discussed have the same sign as the misfit stresses occurring in the film due to the interphase boundary between the substrate and the film. Therefore, the coherent bottom boundary cannot cause relaxation of misfit stresses, in which case the formation of nanograins with coherent bottom boundaries should be energetically unfavourable. (This statement is proved by our calculations; see the next sections.) In this context, we think that the bottom boundaries are incoherent, in which case each boundary contains a delocalized misfit dislocation, that is, a dislocation whose core is spread over the bottom boundary as a whole (figure 3). More precisely, the number n_d of crystallographic planes of the nanograin, matched at the bottom boundary, is different from the number n_m of crystallographic planes of the film matrix. In these circumstances, the incoherent bottom boundary contains a delocalized dislocation with Burgers modulus $B_m = (n_d - n_m)a$. Such a bottom boundary plays the role of a source of dilatation misfit stresses, characterized by the effective misfit parameter

$$\tilde{f}_1 = f_1 - \frac{B_m}{2L}. \tag{3}$$

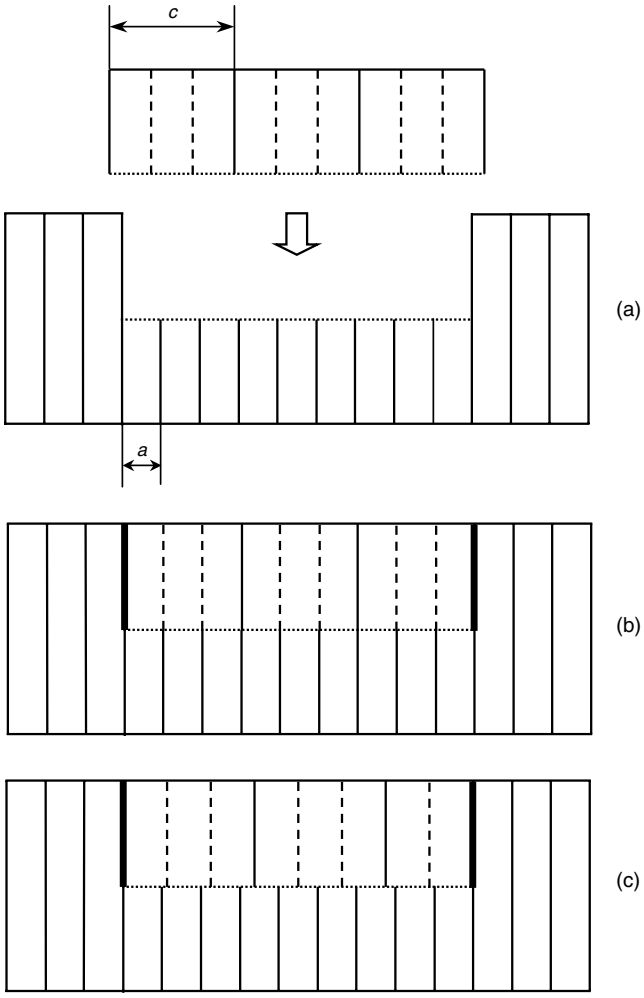

Figure 2. The matching of atomic layers at the bottom 90° tilt boundary of a nanograin. (a) No-matching (imaginary) state. (b) Coherent matching gives rise to compressive stresses in the nanograin. (c) Incoherent matching (with delocalized dislocation) gives rise to tensile stresses in the nanograin.

The parameters f_1 and $\tilde{f}_1$ can have opposite signs, in which case the bottom nanograin boundary creates the elastic stresses compensating, in part, for the misfit stresses occurring at the film/substrate boundary. In doing so, the formation of nanograins with 90° grain boundaries represents a mechanism for relaxation of misfit stresses in strained films.

Thus, in the framework of the suggested model, nanograins in a high-T_c superconducting film have bottom grain boundaries with delocalized misfit dislocations and coherent lateral boundaries. The 90° grain boundaries with delocalized dislocations are stress sources modelled as boundaries with continuously distributed coherent dislocations whose density and infinitesimal Burgers vectors are related to the corresponding effective misfit parameters in accordance with formula (2), where f_1 is replaced by $\tilde{f}_1$. Lateral grain boundaries of nanograins are treated to be coherent boundaries serving as stress sources characterized by the effective misfit parameter $\tilde{f}_2 = -f_1$. To summarize, in the framework of our model, bottom and lateral

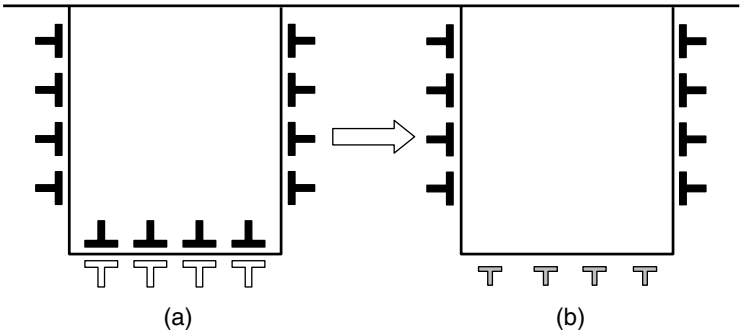

Figure 3. (a) The bottom 90° tilt boundary of a nanograin contains continuously distributed coherent and a delocalized misfit dislocations represented as an ensemble of dislocations (open dislocation signs) with infinitesimal Burgers vectors. (b) The superposition of coherent and delocalized dislocations is represented as an ensemble of continuously distributed dislocations (shaded dislocation signs) with the stress fields compensating, in part, for the misfit stresses generated at the film/substrate boundary.

90° tilt boundaries of nanograins are represented as ensembles of continuously distributed dislocations, whose densities ρ_1 and ρ_2, respectively, are in the following relationships with the effective and conventional misfit parameters:

$$\rho_1\,\mathrm{d}b_1 = \tilde{f}_1 = f_1 - \frac{B_\mathrm{m}}{2L}, \qquad \rho_2\,\mathrm{d}b_2 = \tilde{f}_2 = -f_1. \tag{4}$$

The dislocations characterized by the density ρ_1 at the bottom boundaries of nanograins create stress fields compensating, in part, for the misfit stresses occurring at the film/substrate boundary.

3. Stress fields of a nanograin in a thin solid film

With the representation of the 90° boundaries of a nanograin as rows of continuously distributed misfit dislocations of edge type (see the previous section), here we will calculate the stress field of the nanograin as a superposition of the stress fields created by these misfit dislocations. The stress tensor components for an edge dislocation located at the line ($x = x_0$, $y = 0$) near the free surface are written in the coordinate system shown in figure 1 as follows:

$$\sigma_{ij}^{(b)}(x, y, x_0) = \sigma_{ij}^{(b_x)} + \sigma_{ij}^{(b_y)} + \sigma_{ij}^{(b_z)}. \tag{5}$$

Here $\sigma_{ij}^{(b_k)}$ is the contribution of the kth component of the dislocation Burgers vector ($\boldsymbol{b} = b_k \boldsymbol{e}_k$, $k = x, y, z$) to the stress tensor. In our case, the components $\sigma_{ij}^{(b_z)} = 0$, while the others are given as [40]

$$\sigma_{xx}^{(b_x)} = \frac{Gb_x}{4\pi(1-\nu)}\left(-2\frac{y}{r_1^2} - 4\frac{x_1^2 y}{r_1^4} + 2\frac{y}{r_2^2} + 4\frac{x_2^2 y}{r_2^4} - 2x_0\left[4\frac{x_2 y}{r_2^4} - 16\frac{x_2^3 y}{r_2^6} - 2x_0\left(2\frac{y}{r_2^4} - 8\frac{x_2^2 y}{r_2^6}\right)\right]\right), \tag{6}$$

$$\sigma_{yy}^{(b_x)} = \frac{Gb_x}{4\pi(1-\nu)}\left(-2\frac{y}{r_1^2} + 4\frac{x_1^2 y}{r_1^4} + 2\frac{y}{r_2^2} - 4\frac{x_2^2 y}{r_2^4} - 2x_0\left[-12\frac{x_2 y}{r_2^4} + 16\frac{x_2^3 y}{r_2^6} + 2x_0\left(2\frac{y}{r_2^4} - 8\frac{x_2^2 y}{r_2^6}\right)\right]\right), \tag{7}$$

$$\sigma_{xy}^{(b_x)} = \frac{Gb_x}{4\pi(1-\nu)}\left(-2\frac{x_1}{r_1^2} + 4\frac{x_1^3}{r_1^4} + 2\frac{x_2}{r_2^2} - 4\frac{x_2^3}{r_2^4} - 2x_0\left[\frac{2}{r_2^2} - 16\frac{x_2^2}{r_2^4} + 16\frac{x_2^4}{r_2^6} + 2x_0\left(6\frac{x_2}{r_2^4} - 8\frac{x_2^3}{r_2^6}\right)\right]\right), \tag{8}$$

$$\sigma_{zz}^{(b_x)} = \nu(\sigma_{xx}^{(b_x)} + \sigma_{yy}^{(b_x)}), \tag{9}$$

$$\sigma_{xx}^{(b_y)} = \frac{Gb_y}{4\pi(1-\nu)}\left(-2\frac{x_1}{r_1^2} + 4\frac{x_1^3}{r_1^4} + 2\frac{x_2}{r_2^2} - 4\frac{x_2^3}{r_2^4} + 2x_0\left[-\frac{2}{r_2^2} - 8\frac{x_2^2}{r_2^4} + 16\frac{x_2^4}{r_2^6} + 2x_0\left(6\frac{x_2}{r_2^4} - 8\frac{x_2^3}{r_2^6}\right)\right]\right), \tag{10}$$

$$\sigma_{yy}^{(b_y)} = \frac{Gb_y}{4\pi(1-\nu)}\left(6\frac{x_1}{r_1^2} - 4\frac{x_1^3}{r_1^4} - 6\frac{x_2}{r_2^2} + 4\frac{x_2^3}{r_2^4} + 2x_0\left[-\frac{2}{r_2^2} + 16\frac{x_2^2}{r_2^4} - 16\frac{x_2^4}{r_2^6} - 2x_0\left(6\frac{x_2}{r_2^4} - 8\frac{x_2^3}{r_2^6}\right)\right]\right), \tag{11}$$

$$\sigma_{xy}^{(b_y)} = \frac{Gb_y}{4\pi(1-\nu)}\left(-2\frac{y}{r_1^2} + 4\frac{x_1^2 y}{r_1^4} + 2\frac{y}{r_2^2} - 4\frac{x_2^2 y}{r_2^4} + 2x_0\left[-4\frac{x_2 y}{r_2^4} + 16\frac{x_2^3 y}{r_2^6} + 2x_0\left(2\frac{y}{r_2^4} - 8\frac{x_2^2 y}{r_2^6}\right)\right]\right), \tag{12}$$

$$\sigma_{zz}^{(b_y)} = \nu(\sigma_{xx}^{(b_y)} + \sigma_{yy}^{(b_y)}). \tag{13}$$

Here G denotes the shear strength, ν the Poisson ratio, $x_1 = x - x_0$, $x_2 = x + x_0$ and $r_n^2 = x_n^2 + y^2$, $n = 1, 2$.

The sum stress field $\sigma_{ij}^{(1d)}$ of the dislocation ensemble (figure 3) can be divided into the three terms corresponding to three 90° boundaries of the nanograin:

$$\sigma_{ij}^{(1d)} = \sigma_{ij}^{(1)} + \sigma_{ij}^{(2)} + \sigma_{ij}^{(3)}, \tag{14}$$

where 1, 2, and 3 are indices of the bottom, left and right boundaries of the nanograin shown in figure 3. Dislocations are continuously distributed along these boundaries. The dislocations at the bottom boundary have Burgers vectors with the only one non-zero component b_y. The dislocations at the lateral (left and right) boundaries are characterized by Burgers vectors having the only one non-zero component b_x. In these circumstances, the terms on the right-hand side of formula (14) are effectively calculated using the following formulae:

$$\sigma_{ij}^{(1)} = \int_{-L}^{L} \rho_1 \sigma_{ij}^{(b_y)}(x, y - y_0, x_0 = h)\,\mathrm{d}y_0, \tag{15}$$

$$\sigma_{ij}^{(2)} = -\int_{0}^{h} \rho_2 \sigma_{ij}^{(b_x)}(x, y + L, x_0)\,\mathrm{d}x_0, \tag{16}$$

$$\sigma_{ij}^{(3)} = \int_{0}^{h} \rho_2 \sigma_{ij}^{(b_x)}(x, y - L, x_0)\,\mathrm{d}x_0. \tag{17}$$

With formulae (6)–(13) for the dislocation stress tensor components and condition (4), from formulae (15)–(17) we find the stress tensor components characterizing a nanograin (figure 1) in the thin solid film to be as follows:

$$\sigma_{xx}^{(1d)} = \frac{G}{2\pi(1-\nu)}\left\{(\tilde{f}_1 + \tilde{f}_2)x_1\left(\frac{y_2}{A_{12}} - \frac{y_1}{A_{11}}\right) + [(\tilde{f}_2 - \tilde{f}_1)x_1 + 2\tilde{f}_2 x_2]\left(\frac{y_2}{A_{22}} - \frac{y_1}{A_{21}}\right) - 4\tilde{f}_2 x\left(\frac{y_2}{A_2} - \frac{y_1}{A_1}\right) + 4(\tilde{f}_1 + \tilde{f}_2)hxx_2\left(\frac{y_2}{A_{22}^2} - \frac{y_1}{A_{21}^2}\right)\right.$$

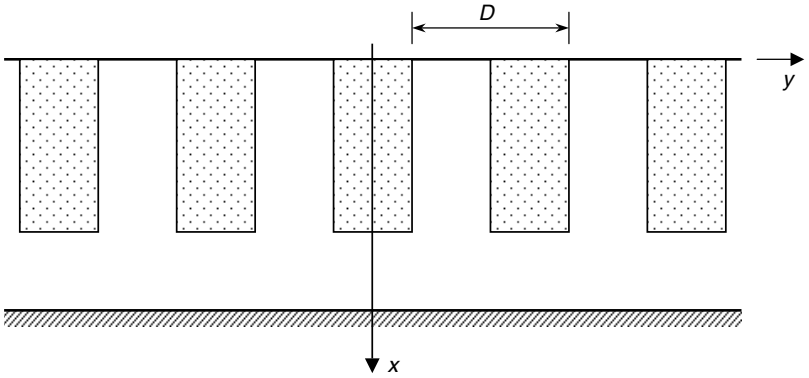

Figure 4. The periodic arrangement of identical nanograins in solid film.

$$+ 2\tilde{f}_2\left[2\left(\arctan\frac{x}{y_2} - \arctan\frac{x}{y_1}\right) - \arctan\frac{x_1}{y_2} + \arctan\frac{x_1}{y_1} - \arctan\frac{x_2}{y_2} + \arctan\frac{x_2}{y_1}\right]\Bigg\}, \tag{18}$$

$$\sigma_{yy}^{(1d)} = \frac{G}{2\pi(1-\nu)}\Bigg\{-(\tilde{f}_1+\tilde{f}_2)x_1\left(\frac{y_2}{A_{12}} - \frac{y_1}{A_{11}}\right) + [(\tilde{f}_1 - 3\tilde{f}_2)x_1 + 4\tilde{f}_1 h]\left(\frac{y_2}{A_{22}} - \frac{y_1}{A_{21}}\right) + 4\tilde{f}_2 x\left(\frac{y_2}{A_2} - \frac{y_1}{A_1}\right) - 4(\tilde{f}_1+\tilde{f}_2)hxx_2\left(\frac{y_2}{A_{22}^2} - \frac{y_1}{A_{21}^2}\right) + 2\tilde{f}_1\left[\arctan\frac{y_2}{x_1} - \arctan\frac{y_1}{x_1} - \arctan\frac{y_2}{x_2} + \arctan\frac{y_1}{x_2} - \arctan\frac{x_2}{y_2} + \arctan\frac{x_2}{y_1}\right] + 4\tilde{f}_2\left[\arctan\frac{x}{y_2} - \arctan\frac{x}{y_1} - \arctan\frac{x_2}{y_2} + \arctan\frac{x_2}{y_1}\right]\Bigg\}, \tag{19}$$

$$\sigma_{xy}^{(1d)} = \frac{G}{2\pi(1-\nu)}\Bigg\{-(\tilde{f}_1+\tilde{f}_2)x_1^2\left(\frac{1}{A_{12}} - \frac{1}{A_{11}}\right) + 4\tilde{f}_2 x^2\left(\frac{1}{A_2} - \frac{1}{A_1}\right) + [(\tilde{f}_1+\tilde{f}_2)x_2^2 + 2(\tilde{f}_1 - \tilde{f}_2)hx - 4\tilde{f}_2 x^2]\left(\frac{1}{A_{22}} - \frac{1}{A_{21}}\right) - 4(\tilde{f}_1+\tilde{f}_2)hxx_2^2\left(\frac{1}{A_{22}^2} - \frac{1}{A_{21}^2}\right) + \frac{1}{2}(\tilde{f}_1 - \tilde{f}_2)\left[\ln\frac{A_{12}}{A_{22}} - \ln\frac{A_{11}}{A_{21}}\right]\Bigg\}, \tag{20}$$

$$\sigma_{zz}^{(1d)} = \nu(\sigma_{xx}^{(1d)} + \sigma_{yy}^{(1d)}), \qquad \sigma_{xz}^{(1d)} = \sigma_{yz}^{(1d)} = 0. \tag{21}$$

Here $x_1 = x - h$, $x_2 = x + h$, $y_1 = y - L$, $y_2 = y + L$, $A_{mn} = x_m^2 + y_n^2$ and $A_n = x^2 + y_n^2$ $(m, n = 1, 2)$.

In general, real films can contain many nanograins. For instance, in experiments [25], the volume fraction of film regions occupied by nanograins reaches 40%. The nanograins as stress sources elastically interact, in which case the energy of elastic interaction between nanograins contributes to the total energy of the film with nanograins. Let us consider a model film with an infinite row of periodically arranged (with period D) identical nanograins (figure 4). The stress created by such nanograins can be represented as the following infinite sum:

$$\sigma_{ij}^{(d)} = \sum_{n=-\infty}^{\infty} \sigma_{ij}^{(1d)}(x, y - nD). \tag{22}$$

After summation of expression for stresses (18)–(21), we find

$$\sigma_{xx}^{(\mathrm{d})} = \frac{G}{2\pi(1-\nu)}\left\{\frac{1}{2}(\tilde{f}_1+\tilde{f}_2)X_1\left(\frac{\sin Y_2}{P_{12}}-\frac{\sin Y_1}{P_{11}}\right)-2\tilde{f}_2X\left(\frac{\sin Y_2}{P_2}-\frac{\sin Y_1}{P_1}\right)\right.$$
$$+\frac{1}{2}[(\tilde{f}_2-\tilde{f}_1)X_1+2\tilde{f}_2X_2]\left(\frac{\sin Y_2}{P_{22}}-\frac{\sin Y_1}{P_{21}}\right)$$
$$+(\tilde{f}_1+\tilde{f}_2)\tilde{h}X\sinh X_2\left(\frac{\sin Y_2}{P_{22}^2}-\frac{\sin Y_1}{P_{21}^2}\right)$$
$$+2\tilde{f}_2\Bigg[2(\arctan Q_1-\arctan Q_2)+\arctan Q_{12}$$
$$-\arctan Q_{11}+\arctan Q_{22}-\arctan Q_{21}$$
$$+\frac{\pi}{2}(1-\operatorname{sgn}(x-h))\sum_{n=-\infty}^{+\infty}\Bigg[\operatorname{sgn}(y+nd+L)-\operatorname{sgn}(y+nd-L)$$
$$+\operatorname{sgn}\left(-\frac{d}{2}-y-nd\right)-\operatorname{sgn}\left(-\frac{d}{2}+L-y-nd\right)+\operatorname{sgn}\left(y+nd-\frac{d}{2}\right)$$
$$\left.-\operatorname{sgn}\left(y+nd-\frac{d}{2}+L\right)\Bigg]\Bigg]\right\}, \tag{23}$$

$$\sigma_{yy}^{(\mathrm{d})} = \frac{G}{2\pi(1-\nu)}\left\{-\frac{1}{2}(\tilde{f}_1+\tilde{f}_2)X_1\left(\frac{\sin Y_2}{P_{12}}-\frac{\sin Y_1}{P_{11}}\right)+2\tilde{f}_2X\left(\frac{\sin Y_2}{P_2}-\frac{\sin Y_1}{P_1}\right)\right.$$
$$+\frac{1}{2}[(\tilde{f}_1-3\tilde{f}_2)X_1+4\tilde{f}_1\tilde{h}]\left(\frac{\sin Y_2}{P_{22}}-\frac{\sin Y_1}{P_{21}}\right)$$
$$-(\tilde{f}_1+\tilde{f}_2)\tilde{h}X\sinh X_2\left(\frac{\sin Y_2}{P_{22}^2}-\frac{\sin Y_1}{P_{21}^2}\right)$$
$$+2\tilde{f}_1\Bigg(\arctan Q_{12}-\arctan Q_{11}-\arctan Q_{22}+\arctan Q_{21}$$
$$+\frac{\pi}{2}(1-\operatorname{sgn}(x-h))\sum_{n=-\infty}^{+\infty}\Bigg[\operatorname{sgn}\left(-\frac{d}{2}-y-nd\right)-\operatorname{sgn}\left(-\frac{d}{2}+L-y-nd\right)$$
$$+\operatorname{sgn}\left(y+nd-\frac{d}{2}\right)-\operatorname{sgn}\left(y+nd-\frac{d}{2}+L\right)\Bigg]\Bigg)$$
$$\left.+4\tilde{f}_2(\arctan Q_1-\arctan Q_2+\arctan Q_{22}-\arctan Q_{21})\right\}, \tag{24}$$

$$\sigma_{xy}^{(\mathrm{d})} = \frac{G}{2\pi(1-\nu)}\left\{\frac{1}{2}(\tilde{f}_2-\tilde{f}_1)\left[\ln\frac{P_{12}}{P_{22}}-\ln\frac{P_{11}}{P_{21}}\right]-\frac{1}{2}(\tilde{f}_1+\tilde{f}_2)X_1\sinh X_1\left(\frac{1}{P_{12}}-\frac{1}{P_{11}}\right)\right.$$
$$+2\tilde{f}_2X\sinh X\left(\frac{1}{P_2}-\frac{1}{P_1}\right)+\frac{1}{2}[\tilde{f}_1X_2+\tilde{f}_2(\tilde{h}-3X)]\left(\frac{1}{P_{22}}-\frac{1}{P_{21}}\right)$$
$$\left.+(\tilde{f}_1+\tilde{f}_2)\tilde{h}X\left(\frac{1-\cosh X_2\cos Y_2}{P_{22}^2}-\frac{1-\cosh X_2\cos Y_1}{P_{21}^2}\right)\right\}, \tag{25}$$

$$\sigma_{zz}^{(\mathrm{d})} = \nu(\sigma_{xx}^{(\mathrm{d})}+\sigma_{yy}^{(\mathrm{d})}), \qquad \sigma_{xz}^{(\mathrm{d})} = \sigma_{yz}^{(\mathrm{d})} = 0. \tag{26}$$

Here $X = 2\pi x/D$, $X_n = 2\pi x_n/D$, $Y_n = 2\pi y_n/D$, $P_{mn} = \cosh X_m - \cos Y_n$, $P_n = \cosh X - \cos Y_n$, $Q_{mn} = \coth(X_m/2)\tan(Y_n/2)$, $Q_n = \coth(X/2)\tan(Y_n/2)$ $(m, n = 1, 2)$. These expressions obey the equations of equilibrium ($\mathrm{div}\sigma_{ij}^{(\mathrm{d})} = 0$) of the elasticity theory and the boundary conditions ($\sigma_{xj}^{(\mathrm{d})}(x = 0, y) = 0$) at the free surface.

4. Energy characteristics of nanograins in high-T_c superconducting film

Let us consider the conditions at which the formation of nanograins in a high-T_c superconducting film is energetically favourable. To do this, we shall compare the energy characteristics of the two physical states realized in the film, namely the state with nanograins and the nanograin-free state. The formation of nanograins is energetically favourable if

$$\Delta W = W_d - W_0 < 0, \tag{27}$$

where ΔW is the difference between the energies of the film with nanograins (W_d) and the nanograin-free film (W_0).

In order to calculate the energies, we consider a model film/substrate system consisting of a thin solid film of thickness H on a semi-infinite substrate. The film and the substrate are assumed to be elastically isotropic solids having the same values of the shear strength G and the same values of Poisson ratio ν. The two-dimensional geometric mismatch at the film/substrate boundary plane is characterized by the misfit parameters $f_a = 2(a_s - a)/(a_s + a)$ and $f_b = 2(b_s - b)/(b_s + b)$, where a and b are the crystal lattice parameters of YBaCuO film in its (a, b)-crystallographic plane matched with the crystal lattice plane of the substrate, characterized by the lattice parameters a_s and b_s, respectively.

In the nanograin-free film, the only uniform misfit stresses exist which are written in the coordinate system shown in figure 3 as follows [24]:

$$\sigma_{yy}^{(f)} = -\frac{2G}{1-\nu}(f_a + \nu f_b), \qquad \sigma_{zz}^{(f)} = -\frac{2G}{1-\nu}(f_b + \nu f_a). \tag{28}$$

Then the elastic energy density (per unit volume) w_0 of the nanograin-free film is given by [24]

$$w_0 = \frac{G}{1-\nu}(f_a^2 + f_b^2 + 2\nu f_a f_b). \tag{29}$$

The energy W_d (per period of the arrangement of nanograins) contains two terms: the elastic energy W_d^{el} of the nanograins and the energy W_γ that characterizes incoherent matching at the bottom boundaries of the nanograins. In other words, W_γ is the energy of the chemical bonds broken at the incoherent bottom boundaries of the nanograins. With γ being the energy density (per unit area) of the incoherent boundary, we have

$$W_\gamma = 2L\gamma. \tag{30}$$

To calculate the elastic energy W_d^{el} of the film with nanograins (figure 4), it is convenient to use the classical expression for the elastic energy density (per unit volume) which is written in its general form [41] as follows:

$$w = \frac{1}{2E}(\sigma_{xx}^2 + \sigma_{yy}^2 + \sigma_{zz}^2) - \frac{\nu}{E}(\sigma_{xx}\sigma_{yy} + \sigma_{yy}\sigma_{zz} + \sigma_{xx}\sigma_{zz}) + \frac{1}{2G}(\sigma_{xy}^2 + \sigma_{yz}^2 + \sigma_{xz}^2). \tag{31}$$

The stresses in this film result from the superposition of the misfit stresses $\sigma_{ij}^{(f)}$ and stresses $\sigma_{ij}^{(d)}$ generated by the nanograins (more precisely, nanograin/film matrix boundaries). That is, the stresses σ_{ij} figuring in formula (31) can be represented as

$$\sigma_{ij} = \sigma_{ij}^{(d)} + \sigma_{ij}^{(f)}. \tag{32}$$

Thus, the formulae in sections 3 and 4 allow us to calculate the characteristic energy difference ΔW (per period of the arrangement of nanograins) written as follows:

$$\Delta W = \int_{-D/2}^{D/2} \mathrm{d}y \int_0^\infty \mathrm{d}x\ (w - w_0) + W_\gamma. \tag{33}$$

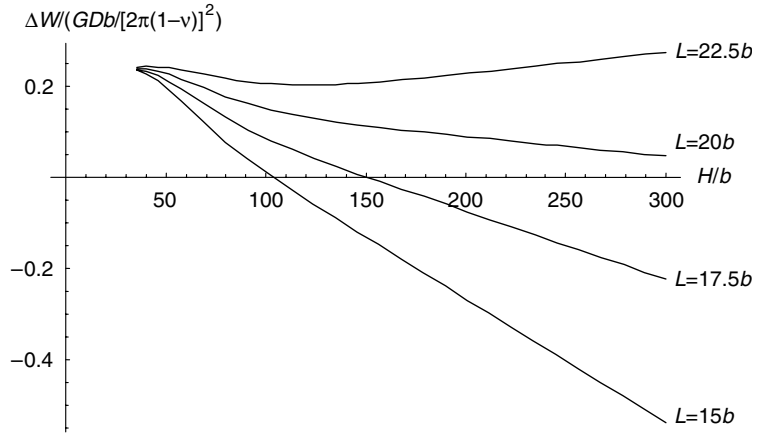

Figure 5. The dependence of the characteristic energy difference ΔW on the film thickness H, for the nanograin height $h = H - 30b$ and different values of the nanograin half-width L.

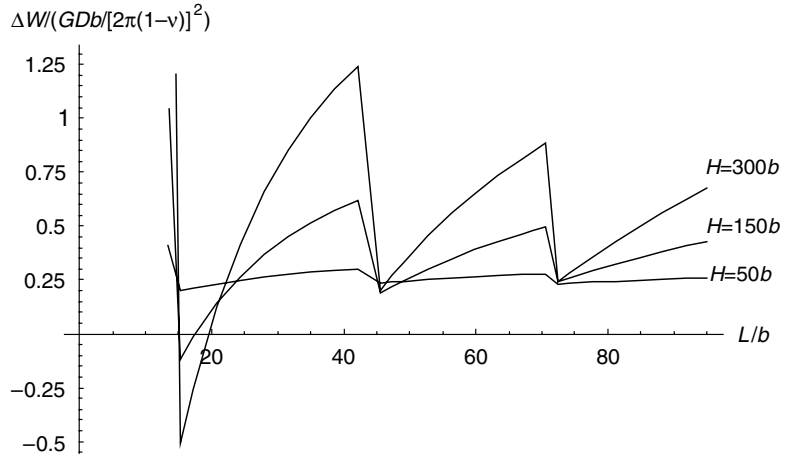

Figure 6. The dependence of the characteristic energy difference ΔW on the nanograin half-width L, for the nanograin height $h = H - 30b$ and different values of the film thickness H.

With formulae (30) and (33), we have calculated ΔW in the exemplary case of $YBa_2Cu_3O_{7-\delta}$ film (deposited onto $LaAlO_3$ substrate) having crystal lattice parameters (for details, see [42]) $a = 0.3824$, $b = 0.3886$ and $c = 1.168$ nm. The incoherent matching at the boundary is similar to that at a stacking fault. With this taken into account, we estimate γ as the stacking fault energy density given as [15]: $\gamma = 24Gb/[324\pi(1-\nu)]$. In our case with $YBa_2Cu_3O_{7-\delta}$, for $G = 55$ GPa and $\nu = 0.26$, we have $\gamma \approx 0.6$ J m^{-2}. According to these calculations, the criterion $\Delta W < 0$ for the formation of nanograins to be energetically favourable is valid in wide ranges of geometric parameters (film thickness H, nanograin sizes h and L) of $YBa_2Cu_3O_{7-\delta}$ film with nanograins. Dependences of ΔW, given by formulae (30) and (33), on the film thickness H and nanograin half-width L are shown in figures 5 and 6, respectively, for the period $D = 5L$ of nanograin arrangement in the film. In experiments [25], the bottom boundaries of nanograins have been observed to be distant by $(30-45)b$ from the film/substrate boundary. Therefore, in our calculations, we have used the nanograin height as $h = H - 30b$.

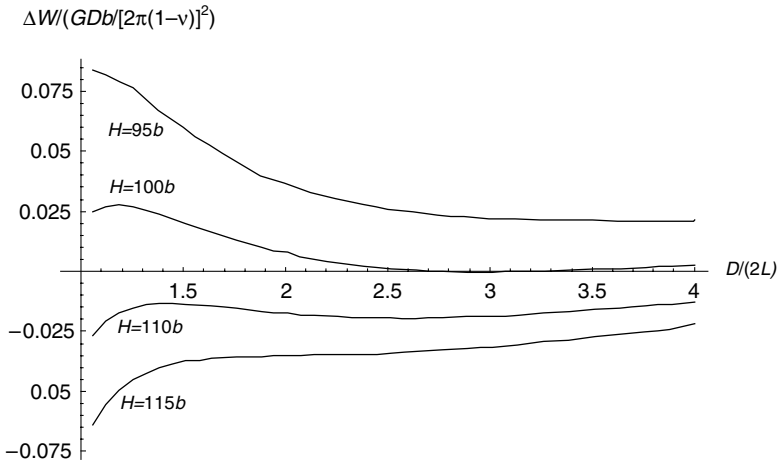

Figure 7. The dependence of the characteristic energy difference ΔW on the period D of the ensemble of nanograins, for $L = 15b$ and different values of the film thickness.

From figure 6 it follows that the characteristic energy difference ΔW is negative only in the narrow range of $L \approx (15 - 20)b$. That is, the nanograin width corresponding to the energetically favourable formation of nanograins is $2L \approx (30 - 40)b$. These values of $2L$ are in agreement with experimental data [25].

The saw-like character of the dependence $\Delta W(L)$ is effectively explained with formula (3) as follows. At low values of L the generation of one delocalized misfit dislocation at the bottom boundary between the nanograin and the film matrix is energetically favourable. With rising L, the effective misfit parameter $\tilde{f}_1$ changes in accordance with formula (3), leading to a gradual increase of ΔW. At some critical value of L, the integrated misfit at the bottom boundary between the nanograin and the film matrix causes the energetically favourable generation of an extra (second) misfit dislocation spread over the bottom boundary as a whole. It leads to a dramatic fall of both the effective misfit parameter $\tilde{f}_1$ and, therefore, the energy difference ΔW at this critical value of L. Further increase of L causes a gradual change of $\tilde{f}_1$ and ΔW, and so on. Thus, the discussed features of the dependence of $\tilde{f}_1$ on L, given by formula (3), give rise to the saw-like character of the dependence $\Delta W(L)$.

The dependences of ΔW on the period D in the arrangement of nanograins in a strained $YBa_2Cu_3O_{7-\delta}$ film are presented in figure 7, for $L = 15b$ and different values of the film thickness H, being in vicinity of the critical value $H_c \approx 100b$ (see figure 5) for the energetically favourable formation of nanograins. For thick films (with thickness $H = 115$ nm), the dependence $\Delta W(D)$ is shown as the lower curve in figure 7. Its monotonic character allows one to conclude that the energetically favourable configuration of nanograins in a thick film is characterized by minimum period $D = 2L$ at which nanograins converge into a continuous layer (figure 7). However, this limiting situation can be realized only at the late stages of the film growth. At the same time, at the early stage of the film growth, nanograins with optimum width ($2L \approx 30 - 40b$) are energetically favourable. In figure 7 is shown the curve of $\Delta W(D)$, for the film thickness $H_c \approx 100b$, which has a pronounced minimum corresponding to the energetically favourable formation of nanograins and giving the volume fraction occupied by these nanograins. For $H = 100b$, the optimum period of nanograin arrangement is $D \approx 5.9L$, in which case the volume fraction in question is about 34%. This is in agreement with experiments [25] showing that the film volume fraction occupied by nanograins is about 40%.

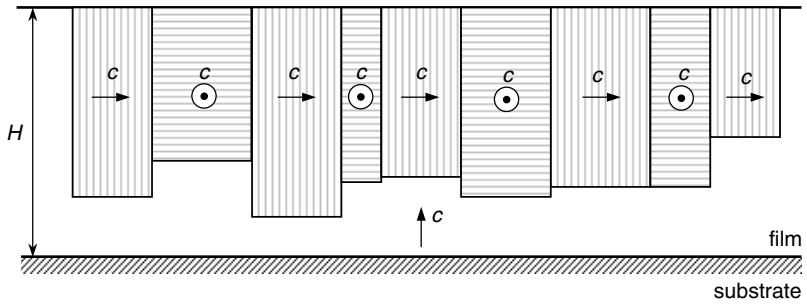

Figure 8. A thick film with a continuous top layer consisting of nanograins of two types with the crystal lattices misoriented by 90° around the *a* and *b* axes relative to the crystal lattice of the film layer adjacent to the film/substrate boundary.

As noted above, in the case of thick films, convergence of nanograins into a continuous layer is energetically favourable. Generally speaking, nanograins can be formed with different misorientations, that is, nanograins with crystal lattices rotated by 90° around axes *a* and *b* relative to the crystal lattice of the film layer adjacent to the film/substrate boundary. They have similar energy characteristics. (In this paper, for definiteness and simplicity, we have focused our consideration only on nanograins of one type.) In a high-T_c cuprate film grown at non-equilibrium conditions, kinetic factors come into play which cause formation of nanograins of different types and having bottom boundaries distant by different spacings from the film/substrate boundary. In these circumstances, the film at late stages of its growth—the thick film—contains a continuous layer consisting of nanograins with alternate, *a*- and *b*-type 90° misorientations (figure 8). Such layers have been observed in experiments [43].

5. Concluding remarks

In this paper a theoretical model has been suggested describing the formation of nanograins with 90° grain boundaries as a new relaxation mechanism in strained high-T_c superconducting films. We have calculated the energy characteristics of nanograins in the exemplary case of $YBa_2Cu_3O_{7-\delta}$ superconducting film growing on $LaAlO_3$ substrate, that has been examined in experiments [25]. In the framework of the model suggested, there are 90° grain boundaries of the two types between the nanograins and the film matrix. At the lateral 90° grain boundaries, the crystal lattices of the film matrix and the nanograins are matched coherently. These crystal lattices are matched incoherently at the bottom 90° grain boundaries, in which case each boundary contains one (or more) delocalized misfit dislocation(s). The bottom boundaries with delocalized dislocation charge serve as stress sources compensating, in part, for the misfit stresses occurring at the film/substrate boundary. Following the results of our theoretical model, their formation in thin $YBa_2Cu_3O_{7-\delta}$ films is energetically favourable in wide ranges of parameters of nanograins. This theoretical statement is in agreement with experimental observation [25] of nanograins in $YBa_2Cu_3O_{7-\delta}$ films.

In this paper we have focused our analysis on YBCO films deposited onto LSAO substrates. However, the results of our consideration can be easily generalized to the situations with cuprate films and substrates with various crystallographic and material characteristics. These results are worth being taken into account in technological applications of high-T_c superconducting films, and in particular, in the design and fabrication of high-T_c superconducting films with grain structure and functional properties regulated by substrate material and film thickness.

Acknowledgments

This work was supported, in part, by the Office of US Naval Research (grants N00014-99-1-0896 and N00014-01-1-1020), the Russian Academy of Sciences and the Russian Foundation of Basic Research (grant 01-02-16853).

References

[1] Dimos D, Chaudhari P, Mannhart J and LeGoues F K 1988 *Phys. Rev. Lett.* **61** 219–22
[2] Dimos D, Chaudhari P and Mannhart J 1990 *Phys. Rev.* B **41** 4038–49
[3] Heinig N F, Redwing R D, Tsu I F, Gurevich A, Nordman J E, Babcock S E and Larbalestier D C 1996 *Appl. Phys. Lett.* **69** 577–9
[4] Locquet J-P, Perret J, Fompeyrine J, Mächler X, Seo J W and van Tendeloo G 1998 *Nature* **394** 453–6
[5] Chisholm M F and Pennycook S J 1991 *Nature* **351** 47–9
[6] Agassi D, Pande C S and Masumura R A 1995 *Phys. Rev.* B **52** 16237–45
[7] Alarco J A and Olsson E 1995 *Phys. Rev.* B **52** 13625–30
[8] Betouras H and Joynt R 1995 *Physica* C **250** 256–64
[9] Hilgenkamp H, Mannhart J and Mayer B 1996 *Phys. Rev.* B **53** 14586–93
[10] Gurevich A and Pashitskii E A 1998 *Phys. Rev.* B **57** 13878–93
[11] Schmehl A, Goetz B, Shulz R R, Schneider C W, Bielefeldt H, Hilgenkamp H and Mannhart J 1999 *Europhys. Lett.* **47** 110–5
[12] Ovid'ko I A 2001 *Mater. Sci. Eng.* A **313** 207–17
[13] Agassi D and Cullen J R 1999 *Physica* C **316** 1–12
[14] Agassi D, Christen D K and Pennycook S J 2002 *Appl. Phys. Lett.* **81** 2803–5
[15] Chisholm M F and Smith D A 1989 *Phil. Mag.* A **59** 181–97
[16] Kung H, Hirth J P, Foltyn S R, Arendt P N, Jia Q X and Maley M P 2001 *Phil. Mag. Lett.* **81** 85–93
[17] Tsu I-F, Babcock S E and Kaiser D L 1996 *J. Mater. Res.* **11** 1383–97
[18] Tsu I-F, Wang J-L, Kaiser D L and Babcock S E 1998 *Physica* C **306** 163–87
[19] Gutkin M Yu and Ovid'ko I A 2001 *Phys. Rev.* B **63** 064515
[20] Bobylev S V and Ovid'ko I A 2003 *Phys. Rev.* B **67** 132506
[21] Ovid'ko I A 2001 *J. Phys.: Condens. Matter* **13** L97–103
[22] Marshall A F and Ramesh R 1994 *Interfaces in High-T_c Superconducting Systems* ed S L Shinde and D A Rudman (New-York: Springer) pp 71–115
[23] Zhang P, Haage T, Habermeier H-U, Kazimirov A, Ruf T and Cardona M 1997 *J. Alloys Compounds* **251** 70–3
[24] Gutkin M Yu and Ovid'ko I A 2002 *J. Phys.: Condens. Matter* **14** 5391–402
[25] Zhai H Y, Rusakova I, Fairhurst R and Chu W K 2001 *Phil. Mag. Lett.* **81** 683–90
[26] Willis J R, Jain S C and Bullough R 1990 *Phil. Mag.* A **62** 115–9
[27] Fitzgerald E A 1991 *Mater. Sci. Rep.* **7** 87–142
[28] van der Merve J H 1991 *Crit. Rev. Solid. State Mater. Sci.* **17** 187–209
[29] Gosling T J, Jain S C, Willis J R, Atkinson A and Bullough R 1992 *Phil. Mag.* A **66** 119–32
[30] Atkinson A and Jain S C 1992 *J. Appl. Phys.* **72** 2242–8
[31] Gosling T J and Willis J R 1994 *Phil. Mag.* A **69** 65–90
[32] Gosling T J, Bullough R, Jain S C and Willi J R 1993 *J. Appl. Phys.* **73** 8267–78
[33] Mobus G, Shummann E, Dehm G and Ruehle M 1995 *Phys. Status Solidi* a **150** 77–87
[34] Jain S C, Harker A H and Cowley R A 1997 *Phil. Mag.* A **75** 1461–515
[35] Ovid'ko I A 1999 *J. Phys.: Condens. Matter* **11** 6521–7
[36] Gutkin M Yu, Ovid'ko I A and Sheinerman A G 2000 *J. Phys.: Condens. Matter* **12** 5391–401
[37] Ovid'ko I A and Sheinerman A G 2001 *J. Phys.: Condens. Matter* **13** 7937–51
Ovid'ko I A and Sheinerman A G 2002 *Phil. Mag.* A **82** 3119–27
Ovid'ko I A and Sheinerman A G 2003 *J. Phys.: Condens. Matter* **15** 2127–35
[38] Ovid'ko I A, Sheinerman A G and Skiba N V 2003 *J. Phys.: Condens. Matter* **15** 1173–81
[39] Plakida N M 1995 *High-Temperature Superconductors* (Berlin: Springer)
[40] Mura T 1968 *Advances in Materials Research* vol 3 (New York: Interscience) pp 1–108
[41] Timoshenko S P and Goodier J N 1970 *Theory of Elasticity* (New York: McGraw-Hill)
[42] Zhai H Y and Chu W K 2000 *Appl. Phys. Lett.* **76** 3469–71
[43] Carim A H and Mitchell T E 1993 *Ultramicroscopy* **51** 228–38